Chemical Physics Letters 766 (2021) 138318

Contents lists available at ScienceDirect

Chemical Physics Letters

journal homepage: www.elsevier.com/locate/cplett

Research paper

The stability of 3C-SiC(1 1 1) on Si(1 1 1) thin films: First-principles calculation

Eric K.K. Abavare [a,*], Bright Kwakye-Awuah [a], Oswald A. Nunoo [a], Peter Amoako-Yirenkyire [b], G. Gebreyesus [d], Abu Yaya [c], Keshaw Singh [a]

[a] Department of Physics, Kwame Nkrumah University of Science and Technology, Kumasi, Ghana
[b] Department of Mathematics, Kwame Nkrumah University of Science and Technology, Kumasi, Ghana
[c] Department of Materials Science and Engineering, University of Ghana, Legon, Ghana
[d] Department of Physics, University of Ghana, Legon, Ghana

A B S T R A C T

We report total energy calculation to elucidate the interface structures between SiC(1 1 1) and Si(1 1 1) with unequal atom densities due to apparent lattice matching between them. The result shows one stable and three metastable structures for a particular interfacial system with energy differences ranging from 10–52 meV per Å^2 for both Si-C and Si-Si interfaces respectively. It was observed that, there is atomic undulation near the Si-C interface pinched at Si substrate. The interface formation energies indicates Si-Si is more favourable compared with Si-C. The electronic structure reveals metallic character due to electron transfer from SiC to Si due to relative electronegativity differences between Si and C atoms.

1. Background

Silicon carbide (SiC) is a semiconductor material with several stacking sequence of carbon and silicon often referred to as polytypism [1] in a long-periodicity. There are several known identifiable polytypic structures with the first six (6) set being the most "basic" and structurally fundamental while the rest, long ranged-periodic[1,2]. The sequential labelling and symmetry are either cubic or hexagonal such as 2*H* (wurtzite), 3*C*(zincblende), 4*H*, 6*H* with the nearest atoms being sp^3 hybridisation. The compounds show rather wide band gap of 2.40, 3.26 and 3.02 eV for 3C-, 4H- and 6H-SiC[3] respectively and their breakdown dielectric strength ten times higher compared with that of Si. These characteristics have received considerable attention as a potential new compound semiconductor materials whose applications in power electronic devices includes but not limited to: Schottky barrier diodes in hostile environment, resistance to radiation damage, chemical stability, biotransducers in biosensors,[4] electro-optical properties of photovoltaics[5] in the visible light region. These applications are plausible because of the material's numerous structural modifications possibilities. In spite of these advantages and impressive volumes of research papers on it in the last 30 years, the realisation of any meaningful technological device application is still a challenge because of lack of reproducibility of high quality large crystal epilayers by sublimation process.

SiC can be employed to grow high quality graphene sheet[6,7] by thermal evaporation of Si atoms from the surfaces of either 4*H*-SiC [8–12] or 6*H*-SiC[13–15] respectively because of similarities in structural symmetry towards mass production of graphene,[16] selective graphitisation of Si atoms from SiC substrates offers natural way to grow few graphene layers on wafer-size pseudosubstrates.[17] Graphene science and graphene technology[18,19] of SiC is an envisaged *de –facto* next generation technology material for device applications.[20,21] The intension of this boom is related to the formation of potential wide area graphene sheets on SiC substrate, a more plausible alternative to the fabrication of large graphene. Nevertheless, the challenge to this expected explosive growth of graphene technology is prevented by the small wafer size of SiC. Therefore, any application usage of this important semiconductor material requires large wafer size. In other to overcome the SiC smallness wafer problem, researchers grow large SiC thin films on Si substrate.[22–25] The epitaxial growth is achieved using chemical vapour deposition which intuitively accommodates the post silicon technology and offer more robust throughput SiC-related device production and application. Notwithstanding, this approach is expected to offer an alternative potential route for large scale synthesis of uniform wafer-size graphene layers for technological application.

It should be noted that SiC on Si substrates growth is only possible for 3C-SiC owning to their inherent intrinsic natural symmetry relationship. But, there is large lattice mismatch that exist between 3C- and Si of

* Corresponding author.
E-mail address: eabavare@yahoo.com (E.K.K. Abavare).

https://doi.org/10.1016/j.cplett.2021.138318
Received 9 November 2020; Received in revised form 9 December 2020; Accepted 2 January 2021
Available online 7 January 2021

about 20 % with bond lengths being 1.88 Å and 2.35 Å, respectively. The growth of 3C-SiC(1 1 1) films on Si(110) surface by chemical vapor deposition has been reported by Nishiguchi and collaborators in which the near interface is smooth.[26] It was observed that there exist geometrical relationship between Si(110) and 3C-SiC(1 1 1) heterostructure which is parallel in the lateral plane, similarly Si[$\bar{1}$ 1 0] is parallel to 3C-SiC[$\bar{1}$ 1 0]. It has been confirmed by other studies that epitaxial growth of 3C-SiC(1 1 1) films on Si can lead to the generation of graphene and often referred to as graphene on silicon (GOS).[27–30] Recently, several groups have employed experimental techniques to investigate the epitaxial graphene growth of 3C-SiC(1 1 1) on Si(1 1 1) substrates[17,31–33] leading to the growth of pseudomorphic SiC thin films in several orders of nanometers on Si.

Nishiguchi group observed that Si lattice constant a_{Si} [001] matches half of the SiC lattice constant a_{SiC}[$\bar{1}\bar{1}$2] with reduced mismatch of 1.66%. Similarly doubling the lattice constant of Si along a_{Si}[$\bar{1}$ 1 0] direction matches two and half of the lattice constant of SiC along the direction a_{SiC}[$\bar{1}$ 1 0] with mismatch of about 0.26 % between Si(110) and 3C-SiC(1 1 1) surface. Now the reduced mismatch is similar when extended to SiC(1 1 1) on Si(1 1 1) interface where the smallest hexagonal cell size of 4 × 4 of Si(1 1 1) almost matches 5 × 5 of SiC(1 1 1) respectively leading to a mismatch of 0.21% which we assumed to be matched. However, the unusual matching can cause epitaxial growth on each of the (1 1 1) faces even though the faces do not meet exactly with each other in terms of facial atomic density. For this reason, the Si(1 1 1) on 3C-SiC(1 1 1) surface with a particular alignment as indicated in Fig. 1 is associated with different interfacial atom densities leading to bond strains and twisting of dangling bonds mainly because of atoms inequality on the two materials surfaces. The matching interface is unusual and can therefore lead to faceting of small surface of different Miller-indeces.[34] As a consequence, whenever a crystal is cut normal to any selected direction randomly, spontaneous polarisation near the interface would results and accelerate the faceting process. If the surface is terminated, it would become unstable and ultimately determines the physical and chemical properties of the structure.[35] Thin film of SiC grown experimentally on Si(110) and Si(1 1 1) terminated surfaces suggest clearly planar interfacial surfaces[26,30] following graphene sublimation on the heterostructure.[31] Clearly, it is scientifically and technologically interesting to examine why the denser SiC(1 1 1) surface grows on sparser Si(1 1 1). The atomistic understanding of clarifying why it is unusual for such lattice matched interfacial morphology to exist is totally unknown and theoretical understanding is required. The motivation of this present work is to employ first-principles calculations in the framework of density functional theory to investigate the atomic structures and electronic states of the interface as well as the structural stability of the heterostructure. The calculation revealed that, near perfect interface exist between the dense 3C-SiC(1 1 1) and relatively sparsed Si(1 1 1) surfaces, indicating an epitaxial growth unlike the situation of the Si(110) on Si(1 1 1) calculation where the interface experiences an undulation[36].

The organisation of the paper is as follows: In Section 2, we describe method of calculation in density functional theory in the framework of real space formalism. Section 3, presents the energetics and construction mechanism of 3C-Si(1 1 1) on Si(1 1 1) interfacial heterostructure, electron states at the interfaces as well as electronic band structures. We summarise our results and give our conclusion in Section 4.

2. Method of calculations

2.1. The density functional theory scheme in real space

The total-energy electronic structure calculations in the framework of density-functional theory has been performed in real space scheme.[37,38] The exchange–correlation effects are treated within the local density approximation (LDA) with parameterized form by Perdew and Zunger[39] fitted to the Quantum Monte Carlo results for the electron gas.[40] Nuclei and core electrons are simulated by norm-conserving pseudopotentials generated in a recipe proposed by Troullier and Martins.[41] We treat the non-local part of the pseudopotentials following the scheme by Kleinman and Bylander.[42] We regard 2*s* and 2*p* of C as well as 3*s* and 3*p* of Si as valence orbitals. We have examined the transferability of the pseudopotentials by generating various core radii and computing structural parameters of 3C-SiC. We found that using core radii of 1.50 a_0 and 1.54 a_0 for 2*s* and 2*p*, respectively, and 2.25 a_0 for both 3*s* and 3*p* (a_0 = 1 bohr = 0.529 Å) yield equilibrium parameters such as lattice constant and bulk modulus of 3C-SiC, which are reproduced within 1 % and 9 % respectively in calculation errors when compared with experimental values accordingly with other LDA calculations[43–45].

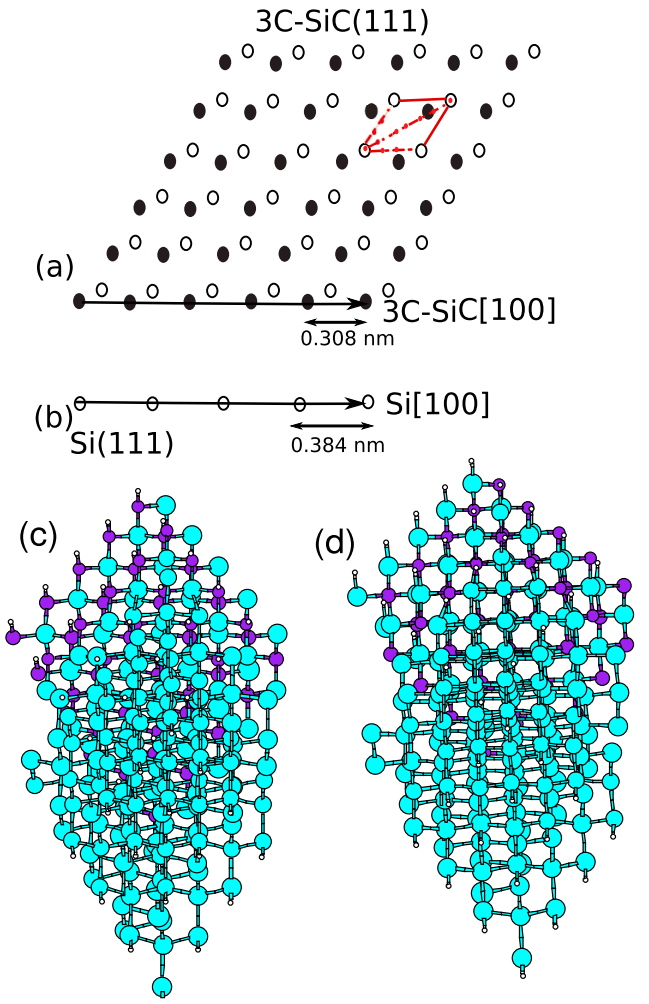

Fig. 1. Schematic illustration of the hexagonal 5x5 of 3C-SiC(1 1 1) surface (a) and 4x4 of Si (1 1 1) surface (b); (c) and (d) are C-rich and Si-rich terminated surfaces with H passivation respectively for the heterostructures, and are slightly pushed down to show the top terminated surfaces. Solid and open balls shows the first- and second-layer of atoms at the 3C-Si(1 1 1) on Si(1 1 1) interface supercell. The parallelogram cell shown in (a) is same in (b) indicating the matching of the lattice sides of the supercell.

In real space formalism (RS), wave function, electron density, potential field and other important related quantities are calculated discretely on three dimensional physical coordinates as lattice grid points. The Hamiltonian matrix in RS is sparce, so computation is efficient when traversing global communication nodes on all parallel computers. In this formalism,[46–48] the kinetic-energy operator is replaced by a finite-difference operation with sixth-order difference formula, which is sufficient for most applications. Systematic

improvements in the accuracy of calculations are achieved by reducing the grid spacing H. In this work, treatment of Si and C element required the use of $H = 0.21$ Å, corresponding to about 62 Ry in the plane-wave-basis-set. This cutoff energy is sufficient to assure the required accuracy of 26 meV per atom in total-energy difference among geometries. Atoms are fully relaxed until forces acting on each atom is smaller than 50 meV/Å. The numerical calculations are performed in this newly developed code, RSDFT, which is designed for large scale calculations on multi-core massively parallel computers.[49,50] The key benefits of the scheme is that, it is essentially free from Fast Fourier Transform (FFT) which is heavy burden in communications on massively parallel architecture. The above calculation procedure could reproduce the formation energy[51] of 3C-SiC at 0.58 eV in good agreement with experiment at 0.68 eV [52].

2.2. Slab model calculation

We define interface as an imperfection of a perfect crystalline material. For the present system of 3C-SiC(1 1 1) on Si(1 1 1) heterostructure, there are only two possible interfaces. The surface plane of C in SiC which meets Si, is the Si-C interface (this creates a surface of Si referred to as Si-rich surface) whereas the interface of Si-Si, is where the Si in SiC meets the Si (again this creates a surface of C called C-rich surface). We employ the repeating slab model with atomic slab periodically arranged along perpendicular direction to the surface and leaving sufficiently thick vacuum layer which creates the intended interface. We obtained stable geometries having used slab model with fixed atomic layers that are far from the interface. By systematically increasing the atomic layers, we examined the convergence of the interface structure and corresponding interface energy. However, this adopted approach is too simplistic and limited in scope because there exist a large number of spatial degrees of freedom for obtaining realistic structures. One key issue is the separation between the 3C-SiC(1 1 1) face from the surface of the substrates Si(1 1 1) along the perpendicular direction for individual atomic relaxation. Secondly, the relative lateral arrangements of atoms must be overcome since this poses serious computational challenges for treatment of realistic heterostructure.

We have overcome these difficulties and obtained stable structures of sparse Si on dense SiC using thin interface slabs which are feasible and then manually explored all multi-dimensional space degrees of freedom for stable structural geometries. For completeness, we used 2 SiC bi-layers (4-layers) and 4-layers of Si to create the 4L/4L interfacial structure (as shown in Fig. 2) with the other two surfaces facing the opposite direction, sufficient vacuum thickness of about 12Å was created. The (1 1 1) surfaces of SiC and Si dangling bonds were terminated with hydrogen atoms[53]. On Si(1 1 1) surface, we examine several different lateral arrangements and optimised the geometries using calculated forces. Stable geometries were reached from the slab model after which we considered lateral primitive cell [the dashed parallelogram in Fig. 1(a)] and define twelve positions on the Si (1 1 1) surface, the twelve dots are indicated and separated from each other by 1Å along $[\bar{1}\,\bar{1}\,\bar{1}]$and [1 0 0] directions of the SiC side. A given trial geometry which represents a dot is defined as (ix_jy) where (i, j = 0, 1, 2, 3) representing the structures in x-y search space. The interface structure can then be visualised as AxA/BxB (where A and B nearly matched lattices) as lateral cell size of SiC and Si respectively shown in Fig. 1 supercell.

Now, we put reference points each for the twelve positions on the lateral cell of the Si side and perform structural optimisation for all the atoms in the slab. This ensure that lateral rearrangements of the indi-

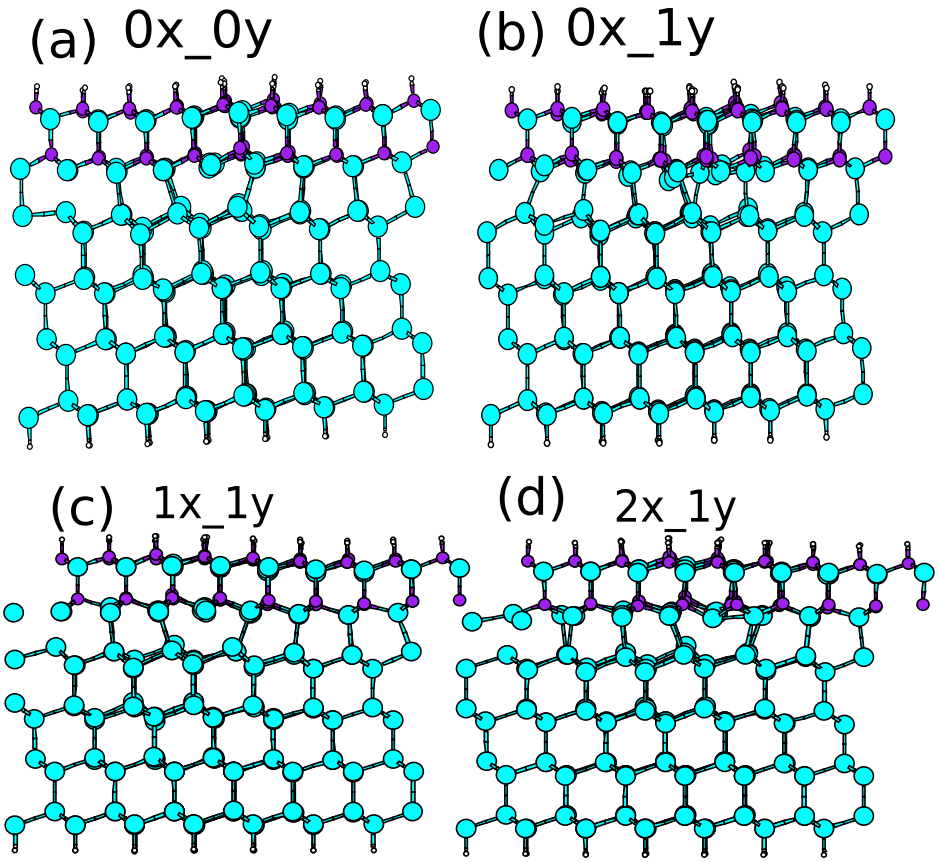

Fig. 2. The side view from Si[1 0 0] direction of the Si substrate or the 3C-Si $[\bar{1}\,\bar{1}\,\bar{1}]$direction of the SiC side geometries: (a) the most stable (S); (b), (c) and (d) Metastable (MS) geometries of Si-Si interface of the 3C-SiC(1 1 1) on Si(1 1 1) heterostructure. The large (blue) and small (purple) balls indicate Si and C atoms respectively. (For interpretation of the references to colour in this figure legend, the reader is referred to the web version of this article.)

vidual atom positions and interfacing spacings are all optimised. This systematic procedure is repeated for all the trial structures. The 3C-SiC (1 1 1) face and Si(1 1 1) faces commensurate to each other in their primitive periodicities, as a consequence, these twelve trials of the structural optimisation inherently includes all the other inequivalent trials in which the reference points in the SiC side is put on somewhere between the twelve selected positions. In this, the search space for the structural optimisation is now expanded. For clarity in the optimization procedure, two stage steps were performed. First, all the atoms in the supercell were allowed to move freely without any constraint including the passivated hydrogen atoms for all the twelve possible structures. Following that exercise, we again repeated the procedure but this time with the hydrogen atoms as well as the first layers of both Si and SiC sides were fixed to mimic the semi-infinite bulk structure of both Si and SiC. After extensive optimisation procedure and calculations, we arrived at four stable structures for Si-C and Si-Si interface each respectively for both two steps approaches which were not dissimilar. Following that, the atomic layers prepared were increased consisting of either 3 or 4 SiC bilayers and 6 or 8 Si layers slabs (8L/8L) successively with terminating H atoms on each geometry. By starting from the optimised structures earlier obtained at the 4L/4L slab model, we relaxed all the atoms in the 8L/8L model slab and those of larger layers were found to be unstable. As a consequence, the rest of the calculations were done using the 4L/4L model heterostructure and the results obtained were not significantly different when compared with the 8L/8L model of earlier calculation of 3C-SiC(1 1 1) on Si(110)[36] system. We found that the calculated interface energies per unit area of the two models were nearly comparable. We found that the interface energy per unit area of the present model with that obtained from 8L/8L of 3C-SiC(1 1 1) on Si(110)[36] interface were comparable. All the performed calculations were done using 2x1x1, ***k***-sampling points in the lateral plane of the Brillouin zone (BZ) region, and this assured the required accuracy of the investigation.

3. Results of calculation and discussion

3.1. Interface relaxation structure

We performed extensive interface geometry calculations of 3C-Si (1 1 1) thin films on Si(1 1 1) substrate, to search for stable structures of either Si-Si or Si-C heterostructure as discussed in Section 2. We found several interface geometries (i.e. four optimised geometries for Si-S and Si-C interfaces respectively). The most stable geometry (S) is the ground state structure while three other metastable geometries(MS) exist. Th atomic arrangements of these stable and metastable structures are shown in Figs. 2 and 3 respectively, with some of the Si-C interfacial atoms showing three- and fivefold coordinated arrangements. Even though 4L/4L interface layers are considered ultra-thin, the interfacial morphology are observed within this regime from previous experience. However, an interesting observation during the investigation is that, beyond the 4L/4L interfacial layers, any additional layer to the

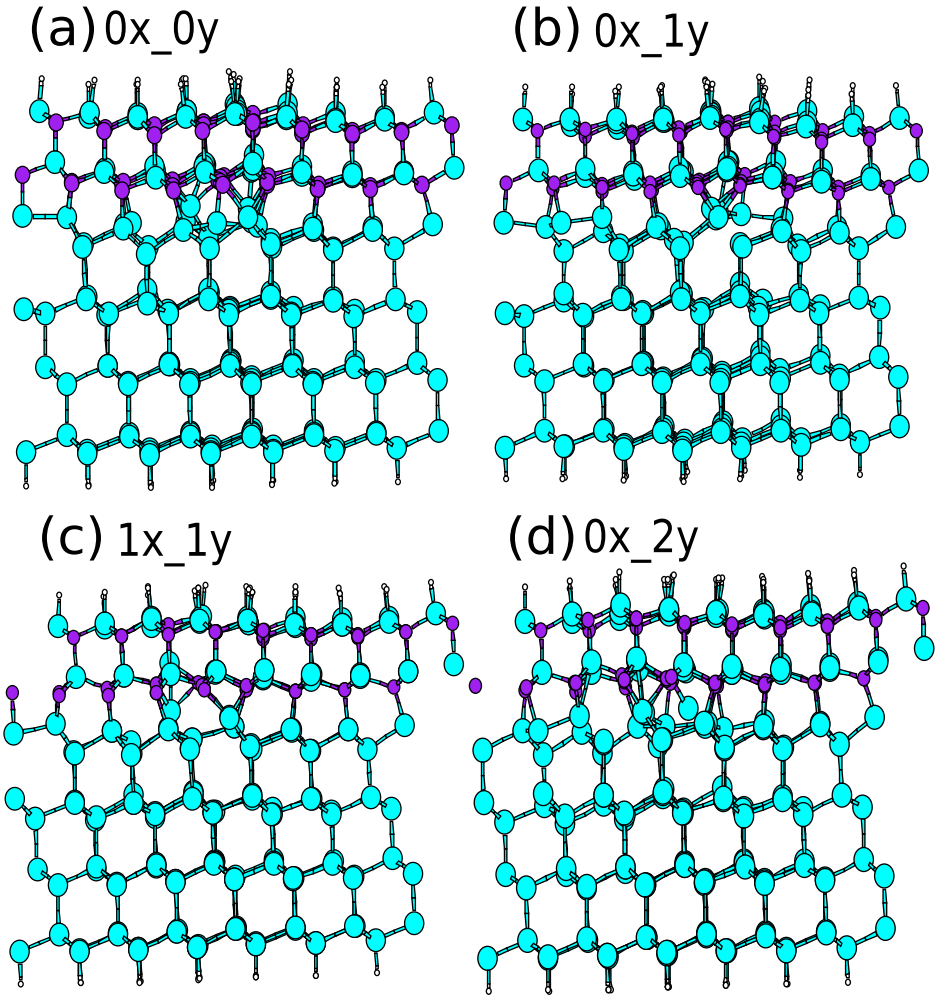

Fig. 3. The side view from Si[1 0 0] direction of the Si substrate or the 3C-Si C[$\bar{1}\,\bar{1}\,\bar{1}$]direction of the SiC side geometries: (b) the most stable (S); (a), (c) and (d) Metastable (MS) geometries of Si-Si interface of the 3C-SiC(1 1 1) on Si(1 1 1) heterostructure. The large (blue) and small (purple) balls indicate Si and C atoms respectively. (For interpretation of the references to colour in this figure legend, the reader is referred to the web version of this article.)

heterostructure rendered the superstructure nearly unstable. We find this situation to be intuitive because, when one ordinarily puts two bulk systems together, it would be clearly unstable and so the interface structures can be thought of in the same way. Therefore, we think of this emergence as a threshold of instability in the geometry beyond which stability breaks-down. The energy differences between MS geometries and S geometry are as follows: 40.94, 6.38 and 51.52 meV/Å^2 respectively as indicated in Fig. 2 for Si-Si interface. Similarly with Si-C interface, we have the MS energies differences being: 2.25, 9.43 and 3.73 meV/Å^2 as referenced in Fig. 3 thereof.

Fig. 4 indicates localised electron charge distribution calculated near the Fermi level for S Si-Si and Si-C interfaces respectively. The charge distributions are floating bonds in character. We find in Fig. 3 that, the Si-C interface has peculiar threefold atomic coordination (dangling bonds) which persist even after the geometry optimisation. The analysis also reveals detailed fivefold coordinated (the floating bonds[54]) appearance of some C atoms at the interface. These under- and over-coordinated atoms creates defects along the Si[0 0 1] or equivalently the SiC[$\bar{1}\,\bar{1}\,\bar{1}$] interface direction.

In Fig. 4, it is evident that, the semblance of combination of these threefold and fivefold coordination bonding mechanism is related to the interface formation stability. This is because there are excess dangling bonds from the SiC side compared with the Si side, which is not one-to-one rebonding hence leading to complex interfacial bonding mechanism as a consequence of atomic mismatch. The revealed fivefold coordinated atoms with floating bonds[54] persisting near the interfaces is uniquely observed in the present situation. As a results, when carefully observed there is an atoms-scale undulation[36] feature appearing near the Si-C interface, making the first interface layer atoms in that region of Si-side to pinched with the SiC and this is not observed at the Si-Si interface. The observed atomic bond distances between the Si and C atoms of the SiC-side are in the range of 1.80–2.08 Å, similarly between the neighbours of Si in the Si-side are 2.29–2.38 Å. When these values are compared with the corresponding bulk bond lengths of 1.89 Å for Si-C and 2.35 Å for Si-Si are very much consistent. Even though, there are no observable bond breaking near the interface of Si-Si (sparse), that is not what is seen at the SiC-side, as there is severe localised stress at the dense SiC-side. This atomic rearrangement may help in the stabilisation of the heterostructure. The general observation is that, the individual compounds in the heterostructure region retains their natural atomic morphology without loss in character.

3.2. Interface energy and band structure calculations

In this section, the interface structural stability is discussed for the calculated systems under consideration. The energy of the interface E_I is such an important quantity that we defined it as the cost of energy needed to form the interface heterostructure of 3C-SiC on Si using the various chemical potentials of the components. The interface energy of the slab model is thus defined as:

$$E_I = E_{\text{opt}} - \mu_{\text{Si}} N_{\text{Si}} - \mu_{\text{C}} N_{\text{C}} - \mu_{\text{H}} N_{\text{H}} \tag{1}$$

where E_{opt} is a calculated slab total energy of a model. The $N_{\text{Si}}, N_{\text{C}}$ and N_{H} are the numbers for Si, C and H atoms respectively in the slab model where $\mu_{\text{Si}}, \mu_{\text{C}}$ as well as μ_{H} as the corresponding chemical potentials of the individual chemical element. With sufficiently thick Si substrate, the interface would be in equilibrium with SiC films as a result, it is proper to assume that

$$\mu_{\text{Si}} = \mu_{\text{bulk Si}}, \ \mu_{\text{C}} = \mu_{\text{bulk SiC}} - \mu_{\text{bulk Si}}, \tag{2}$$

where $\mu_{\text{bulk Si}}$ and $\mu_{\text{bulk SiC}}$ are calculated for each of the crystalline materials per atom as the cohesive energy namely for Si and 3C-SiC respectively, corresponds to the stoichiometric condition of the SiC thin film. For simplicity, stoichiometric condition(SCM, here after) is used to represent such situations as Si-rich or C-poor. Similarly, when there is precipitate of diamond in SiC films as a consequence of limited Si or excess of C, we refer to such condition as Si-poor or C-rich and so we again define the following expressions for the cohesive energies.

$$\mu_{\text{C}} = \mu_{\text{bulk diamond}}, \ \mu_{\text{Si}} = \mu_{\text{bulk SiC}} - \mu_{\text{bulk diamond}}, \tag{3}$$

where $\mu_{\text{bulk diamond}}$ is the cohesive energy of crystalline C per atom.

Now, we need to be extremely careful defining the hydrogen chemical potential μ_{H} in the model system. This is because, in a situation where we simulate Si-C interface, we attache H atoms to Si surface atoms at both sides in the supercell. This means, we must removed all the interface energy contributions originating from H-Si bonding. Therefore, it is appropriate to write the following equation:

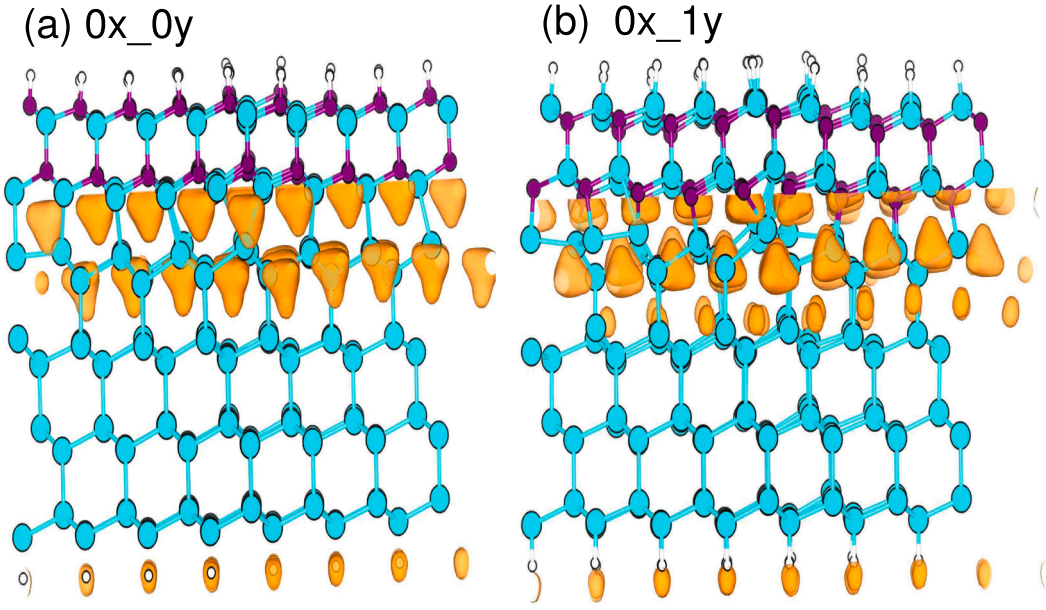

Fig. 4. (Color online) The calculated localised electron distribution near the Fermi level are shown in the Si[0 0 1] or the SiC[$\bar{1}\,\bar{1}\,\bar{1}$] direction of the stable structures of Si-Si (a) and Si-C (b) interfaces respectively. The localised density is indicated by isovalue surface of 35% of the maximum isovalue. The large (blue) and (small) purple balls depicts atoms of Si and C. (For interpretation of the references to colour in this figure legend, the reader is referred to the web version of this article.)

$$\mu_H = \mu_{H(Si)} \equiv (\mu_{Silane} - \mu_{Si})/4. \quad (4)$$

Similarly when Si-Si interface is simulated, we encounter two types of H that needs to be treated differently. That is, those hydrogen atoms attached to the Si surface (top layer) and the others that are with the C surface (bottom layer), their contributions to the interface energy must equally be removed. When hydrogen is attached to Si, we employ Eq. (4) to determine the corresponding chemical potential. The contribution of interface energy coming from C-H bonding and therefore, the corresponding chemical potential of H is defined by the equation below:

$$\mu_H = \mu_{H(C)} \equiv (\mu_{Methane} - \mu_C)/4. \quad (5)$$

The number N_H in Eq. (1) is modified depending on which interface system is being considered. For clarity and consistency, LDA was employed to calculate all the chemical potentials used in the model slab. Having obtained all the relevant chemical potentials, the interface energy per unit area is given as

$$\gamma = \frac{E_I}{A}, \quad (6)$$

with A being the interface area of the slab model.

The interface energy as defined in Eq. (6) is limited in meaning with respect to the calculated absolute value. This is the cost of energy to create the interface from both the bulk SiC and Si in Si-rich stoichiometric condition (SCM), or in Si-poor condition of SiC bulk diamond with attached H at the boundaries. It is clear now that, the stability of the interface can properly be discussed and that assessment of the interface energy E_I is acceptable. Table 1 and Table 2 provide the interface energies calculated for the stable and metastable structures in the SCM or the Si-poor conditions respectively for the initial trial geometry positions. The results shows unambiguously that Si-Si interfaces is energetically favoured compared with Si-C interface in the S geometry of the Si-rich but not Si-poor conditions. However, the situation is different as the MS geometries appear to have indeterminate interface stability. Nevertheless, the stability might depend on the initial trial geometry of the structures in question and also the growth medium. In an extreme case of the Si-poor condition, interface energy E_I is influenced by the deficiency of Si atoms as a result, the stability appear to favour the Si-C interface of the MS geometry and that also depends on the surface of the substrate. The chemical potentials of hydrogen $\mu_{H(Si)}$ in Eq. (4) and $\mu_{H(C)}$ in Eq. (5) have different values: in the stoichiometric condition $\mu_{H(C)}$ is −15.46 eV similarly in the Si-poor condition it is −15.61 eV in the calculation. Since there is uncertainty in the choice of the hydrogen chemical potential, the interface energies should be considered for: $E_I^{'}$ and $E_I^{''}$, with $\mu_H = \mu_{H(Si)}$ and $\mu_H = \mu_{H(C)}$ respectively and similarly in the Si-poor condition as well. This means, the whole spectrum of μ_H limit has reasonably been covered. In Tables 1 and 2, we showed the calculated $E_I^{'}$ and $E_I^{''}$ of the extreme ends of the spectrum of the interface energy base on the different hydrogen chemical potentials. Clearly, the values obtained from the interface calculation, one can conclude that with the exception of the extreme conditions in which SiC films are of low quality because of diamond precipitates, which of course depends on the initial growth environment, the interface of Si-Si is energetically favourable compared with the interface of Si-C.

The calculated energy bands of 4L/4L geometry is shown in Figs. 5 and 6 for Si-C and Si-Si interfaces respectively for the stable and metastable geometries after complete atomic geometry optimisation. Topographically, the two different sets of interfaces dispersions are strikingly different but all show metallic behaviour even though the exchange correlation employed in the calculation is LDA. Figs. 5(b) and 6(a) indicates band structure of the ground state Si-Si and Si-C interfaces respectively, while the remaining figures represents the corresponding metastable bands. The fermi energy level is set to zero of energy in all the figures. The slight differences in the band structure topology for all the structures probably relates to the initial trial geometry. The calculation reveals an intuitive understanding that, excess dangling bonds still persist at the heterojunction and mainly comes from the dense SiC-side. Therefore, there is net dangling bonds from SiC side after rebonding with those coming from the sparsed Si-side. One can conclude

Table 1
Calculated interface energies E_I of the most stable (S) and metastable (MS) geometries of Si-C and Si-Si interfaces in the stoichiometric Si-rich condition. Similarly, when different hydrogen chemical potentials were used, the $E_I^{'}$ and $E_I^{''}$ interfaces were also calculated and indicated (see text).

Geometry	Si-C	S geometry Si-Si
E_I [eV/cell]	27.69	22.57
γ [eV/Å^2]	0.14	0.22
$E_I^{'}$ [eV/cell]	21.73	20.24
$E_I^{''}$ [eV/cell]	28.29	23.87
Geometry		MS geometry
	1x_1y	1x_1y
E_I [eV/cell]	29.58	30.76
γ [eV/Å^2]	0.15	0.12
$E_I^{'}$ [eV/cell]	23.61	21.52
$E_I^{''}$ [eV/cell]	30.17	25.15
	0x_0y	0x_1y
E_I [eV/cell]	28.14	30.76
γ [eV/Å^2]	0.14	0.15
$E_I^{'}$ [eV/cell]	22.18	28.43
$E_I^{''}$ [eV/cell]	28.74	32.06
	0x_2y	2x_1y
E_I [eV/cell]	28.44	32.870
γ [eV/Å^2]	0.14	0.16
$E_I^{'}$ [eV/cell]	22.47	30.54
$E_I^{''}$ [eV/cell]	29.03	34.18

Table 2
Calculated interface energies E_I of the most stable (S) and metastable (MS) geometries of Si-C and Si-Si interfaces in the Si-poor condition. Similarly, when different hydrogen chemical potentials were used, the $E_I^{'}$ and $E_I^{''}$ interfaces were also calculated and indicated (see text).

Geometry	Si-C	S geometry Si-Si
E_I [eV/cell]	96.19	98.34
γ [eV/Å^2]	0.48	0.49
$E_I^{'}$ [eV/cell]	102.74	94.70
$E_I^{''}$ [eV/cell]	108.71	97.26
Geometry		MS geometry
	1x_1y	1x_1y
E_I [eV/cell]	98.07	99.61
γ [eV/Å^2]	0.49	0.50
$E_I^{'}$ [eV/cell]	104.63	95.98
$E_I^{''}$ [eV/cell]	110.59	98.54
	0x_0y	0x_1y
E_I [eV/cell]	96.65	96.64
γ [eV/Å^2]	0.48	0.53
$E_I^{'}$ [eV/cell]	103.20	102.89
$E_I^{''}$ [eV/cell]	109.16	105.44
	0x_2y	2x_1y
E_I [eV/cell]	96.932	108.64
γ [eV/Å^2]	0.48	0.54
$E_I^{'}$ [eV/cell]	103.49	105.00
$E_I^{''}$ [eV/cell]	109.45	107.56

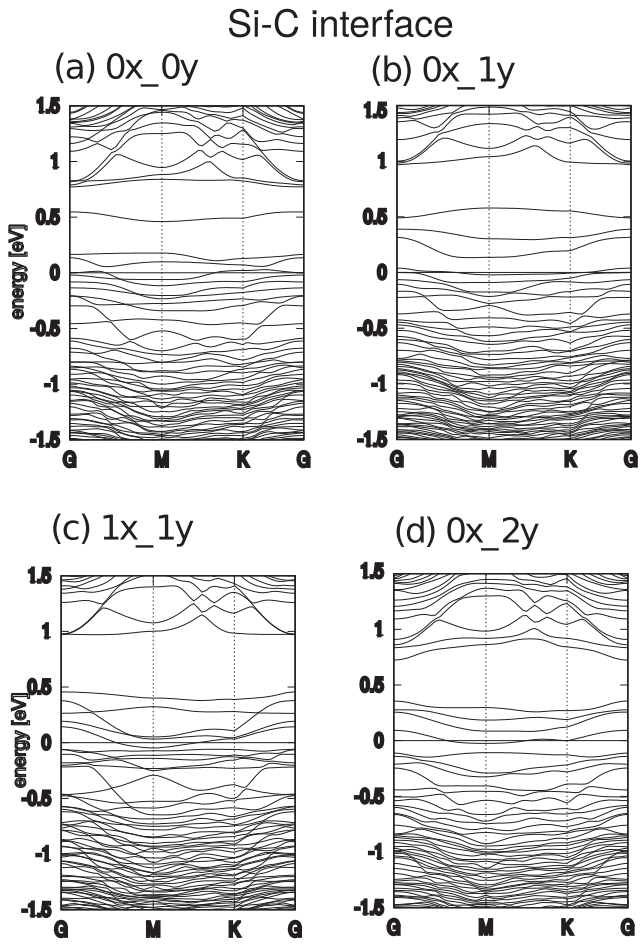

Fig. 5. Calculated optimized band structures of the stable and metastable geometries of Si-C interface (b) stable interface while (a), (c) and (d) indicates metastable interface structures of 3C-SiC(1 1 1) on Si(1 1 1) using the 4L/4L slab model. Fermi level is set as the origin of the energy scale.

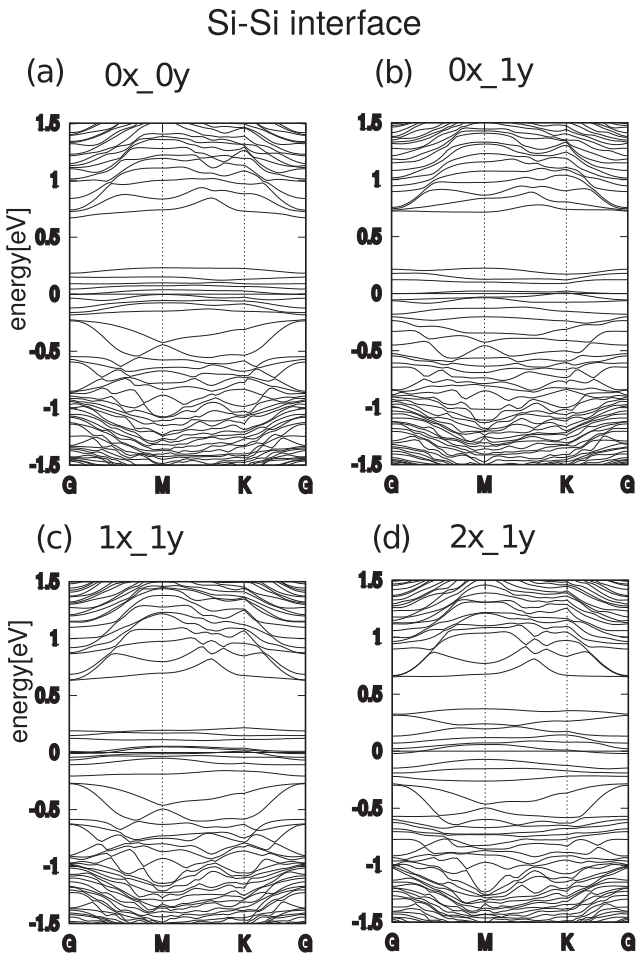

Fig. 6. Calculated optimized band structures of the stable and metastable geometries of Si-Si interface (a) stable interface while (b), (c) and (d) indicates metastable interface structures of 3C-SiC(1 1 1) on Si(1 1 1) using the 4L/4L slab model. Fermi level is set as the origin of the energy scale.

that, the effective unrebonded dangling bonds are the ones giving rise to the metallic behaviour of the interface and this is the consequence of the mismatching atoms of the different compounds forming the interface through twisting and bending bonds. It must be noted that, simple rebonding of the dangling bonds is not possible as relaxation mechanism in the interface is associated with atom-scale undulation especially so for the Si-C interface leading to fivefold coordinated floating bonds. The remaining dangling bonds(under-coordinated atoms) give rise to the metallic character of the interface structures. The electronic distribution relates electron transfer from the SiC side to the Si because of relative differences in electronegativities between Si and C atoms.

4. Conclusion

We report total-energy electronic structure calculations based on density functional theory in the framework of real space formalism. We employed local density approximation and investigated the interface and electronic structures of Si(1 1 1) on 3C-SiC(1 1 1) thin films. The calculations revealed peculia atom scale electronic structure morphologies at the heterojunction as a result of significantly reduced lattice mismatch between the compounds. The differences in atom densities of the two compounds' (1 1 1) surfaces might account for these peculiarities. We have found one stable interface and three other metastable structures each for the investigated interfaces after manually searching all space. The total energy difference between the structures of Si-C and Si-Si interfaces are in the range of 2.25–9.5 meV $Å^2$ and 6–52 meV $Å^2$ respectively with complex electronic bonding mechanism as a results of localised interface states. We find that stable and metastable structures of Si-Si interface are generally epitaxial without any observable bond breaking but bonding strain exist near the heterojunction. However, the Si-C interface is associated with atomic-undulation resulting in over-coordinated atomic bonds which leads to un-expitaxy at the interface and pinched at the Si-region of the Si-C heterojunction. The Si-Si interface energy calculated indicates that, it is energetically favourable compared with that of the Si-C. The electronic band structure calculation of all the interfaces exhibits metallic character for the stable and metastable structures. The origin of metallicity of the heterostructure is due to un-rebonded dangling bonds near the heterojunction because of unequal dangling bonds distribution coming from the denser SiC-region as a result of interfacial atomic mismatch.

CRediT authorship contribution statement

Eric K.K. Abavare: Conceptualization, Data curation, Formal analysis, Investigation, Methodology, Software, Visualization, Supervision, Writing - original draft, Writing - review & editing. **Bright Kwakye-Awuah:** Data curation, Validation, Writing - review & editing. **Oswald A. Nunoo:** Data curation, Resources, Software. **Peter Amoako-Yirenkyire:** Resources, Validation, Visualization, Writing - review & editing. **G. Gebreyesus:** Validation. **Abu Yaya:** Formal analysis, Investigation, Methodology, Resources, Supervision, Writing - review & editing. **Keshaw Singh:** Validation, Supervision, Writing - review &

editing.

Declaration of Competing Interest

The authors declare that they have no known competing financial interests or personal relationships that could have appeared to influence the work reported in this paper.

Acknowledgments

One of us, Eric acknowledges material and logistical support from TWAS under Grant No. 18–027 RG/PHYS/AF/AC_I for scientific research and Kwame Nkrumah University of Science and Technology (KNUST). The authors acknowledge the Centre for High Performance Computing (CHPC), South Africa, for providing computational resources to carry out this scientific research and Prof. Jun-Ich Iwata for the use of RSDFT code.

References

[1] A.R. Verma, P. Krishna, Polymorphism and Polytipism in Crystals, Wiley, New York, 1966.
[2] L.U. Ogbuji, Origin of long-period polytypism in polycrystalline SiC, Phys. stat. sol b 72 (455) (1982) 104–108.
[3] W.E. Nelson, F.A. Halden, A. Rosengren, Growth and properties of -sic single crystals, J. Appl. Phys. 37 (1) (1996) 333–336.
[4] A. Oliveros, A. Guiseppi-Elie, S.E. Saddow, Silicon carbide: a versatile material for biosensor applications, Biomed. Microdivices 2 ((15), 2013,) 353–368.
[5] M. Syväjärvi, Q. Ma, V. Jokubavicius, A. Galeckas, J. Sun, X. Liu, M. Jansson, P. Wellmann, M. Linnarsson, P. Runde, et al., Sol. Energy Mat. Sol. Cells 145 (2016) 104–108.
[6] K.S. Novoselov, A.K. Geim, S. Morozov, D. Jiang, Y. Zhang, S.V. Dubonos, I. V. Grigorieva, A.A. Firsov, Electric field effect in atomically thin carbon films, Science 306 (5696) (2004) 666–669.
[7] K.S. Novoselov, D. Jiang, F. Schedin, T. Booth, V. Khotkevich, S. Morozov, A. K. Geim, Two-dimensional atomic crystals, Proc. Nat. Acad. Sci Mater. 102 (30) (2005) 10451–10453.
[8] C. Riedl, U. Starke, J. Bernhardt, M. Franke, K. Heinz, Structural properties of the graphene-SiC (0001) interface as a key for the preparation of homogeneous large-terrace graphene surfaces, Phys. Rev. B 76 (24) (2007) 245406.
[9] C. Faugeras, A. Nerrière, M. Potemski, A. Mahmood, E. Dujardin, C. Berger, W. De Heer, Few-layer graphene on SiC, pyrolitic graphite, and graphene: a Raman scattering study, Phys. Rev. B 92 (1) (2008) 011914.
[10] J. Hass, J. Millán-Otoya, P. First, E. Conrad, Interface structure of epitaxial graphene grown on 4H-SiC (0001), Phys. Rev. B 78 (20) (2008) 205424.
[11] C. Vecchio, S. Sonde, C. Bongiorno, M. Rambach, R. Yakimova, V. Raineri, F. Giannazzo, Nanoscale structural characterization of epitaxial graphene grown on off-axis 4H-SiC (0001), Nanoscale Res. Lett. 6 (1) (2011) 269.
[12] N.A. Yusof, S.F.A. Rahman, A. Muhammad, Carbon nanotubes and graphene for sensor technology, Synthesis, Techn. and Application of Carbon Nano. (2019) 205–222 Elsevier.
[13] C. Virojanadara, M. Syväjarvi, R. Yakimova, L. Johansson, A. Zakharov, T. Balasubramanian, Homogeneous large-area graphene layer growth on 6 H-SiC (0001), Phys. Rev. B 78 (24) (2008) 245403.
[14] N. Ferralis, R. Maboudian, C. Carraro, Evidence of structural strain in epitaxial graphene layers on 6H-SiC (0001), Phys. Rev. B 101 (14) (2008) 156801.
[15] E. Rollings, G.-H. Gweon, S. Zhou, B. Mun, J. McChesney, B. Hussain, A. Fedoro, P. First, W. De Heer, A. Lanzara, Synthesis and characterization of atomically thin graphite films on a silicon carbide substrate, J. Phys. Chem. Solids 67 (9–10) (2006) 2172–2177.
[16] B. Deng, Z. Liu, H. peng, Toward mass production of CVD graphene films, Adv. Mat. 32 (9) (2019) 1800996.
[17] A. Querghi, M. Marangolo, R. Belkhou, S. El Moussaoui, M. Silly, M. Eddrief, L. Largeau, M. Portail, B. Fain, F. Sirotti, Epitaxial graphene on 3C-SiC (1 1 1) pseudosubstrate: structural and electronic properties, Phys. Rev. B 82 (12) (2010) 125445.
[18] Y.-M. Lin, C. Dimitrakopoulos, K.A. Jenkins, D.B. Farmer, H.-Y. Chiu, A. Grill, P. Avouris, 100-GHz transistors from wafer-scale epitaxial graphene, Sci. 327 (5966) (2010) 662.
[19] A. Venugopal, B.S. Cook, L. Colombo, R.R. Doering, Graphene heterolayers for electronic applications, US. Patent. App. 10/181 (Jan. 15, 2019) 521.
[20] Q. Wang, Q. Tan, Y. Liu, C. Qing, X. Feng, D. Yu, Phys. Status Solidi B 256 (2019) 1900197.
[21] Q. Tan, Q. Wang, Y. Liu, C. Liu, X. Feng, D. Yu, J. Phys.: Condens Matter 30 (8pp) (2018) 305304.
[22] S. Nishino, J.A. Powell, H.A. Will, Production of large-area single-crystal wafers of cubic SiC for semiconductor devices, Appl. Phys. Lett. 42 (5) (1983) 460–462.
[23] S. Nishino, Y. Hazuki, H. Matsunami, T. Tanaka, Chemical vapor deposition of single crystalline -sic films on silicon substrate with sputtered SiC intermediate layer, J. Electrochem. Soc. 127 (12) (1983) 2674–2680.
[24] Q. Wahab, R. Glass, I. Ivanov, J. Birch, J.-E. Sundgren, M. Willander, Growth of epitaxial 3C-SiC films on (1 1 1) silicon substrates at 850°C by reactive magnetron sputtering, J. Appl. Phys. 74 (3) (1993) 1663–1669.
[25] T. Perova, J. Wasyluk, S. Kukushkin, A. Osipov, N. Feoktistov, S. Grudinkin, Micro-Raman mapping of 3C-SiC thin films grown by solid–gas phase epitaxy on Si (111), Nanoscale Res. Lett. 5 (9) (2010) 1507.
[26] T. Nishiguchi, M. Nakamura, K. Nishio, T. Isshiki, S. Nishino, Heteroepitaxial growth of (111) 3C–SiC on well-lattice-matched (110) Si substrates by chemical vapor deposition, Appl. Phys. Lett. 84 (16) (2004) 3082–3084.
[27] M. Suemitsu, Y. Miyamoto, H. Handa, A. Konno, Graphene formation on a 3C-SiC (111) thin film grown on Si (110) substrate, e-journal of Surf, Sci. Nanotech. 7 (9) (2009) 311–313.
[28] M. Suemitsu, H. Fukidome, Epitaxial graphene on silicon substrates, J. Phys. D: Appl. Phys. 43 (37) (2010) 374012.
[29] A. Severino, C. Bongiornor, N. Piluso, M. Italia, M. Camarda, M. Mauceri, G. Condorelli, M. Di Stefano, B. Cafra, A. La Magna, et al., High-quality 6 inch (111) 3C-SiC films grown on off-axis (111) Si substrates, Thin Solid Films 518 (6) (2010) S165–S169.
[30] H. Fukidome, S. Abe, R. Takahashi, K. Imaizumi, S. Inomata, H. Handa, E. Saito, Y. Enta, A. Yoshigoe, Y. Teraoka, et al. Controls over structural and electronic properties of epitaxial graphene on silicon using surface termination of 3C-SiC (1 1 1)/Si, Appl. Phys. Exp. 4 (11) (2011) 115104.
[31] A. Ouerghi, R. Belkhou, M. Marangolo, M. Silly, S. El Moussaoui, M. Eddrief, L. Largeau, M. Portail, F. Sirotti, Structural coherency of epitaxial graphene on 3C–SiC (111) epilayers on Si (111), Appl. Phys. Lett. 97 (16) (2010) 161905.
[32] A. Avramchuk, I. Komissarov, M. Mikhalik, V.Y. Fominski, R. Romanov, A. Sultanov, N. Siglovaya, S. Ryndya, A. Gusev, V. Labunov, et al., IOP Conf. Ser.: Mater. Sci. Eng. 475 (1) (2019) 012036.
[33] R. Suryana, D. Sandi, H. Nakahara, Y. Saito, RHEED patterns of 3 nm carbon layer coated Si (111) surface using Sputtering, J. Phys: Conf. Ser. 1204 (1) (2019) 012112.
[34] R. Tung, A. Levi, J. Sullivan, F. Schrey, Schottky-barrier inhomogeneity at epitaxial NiSi 2 interfaces on Si (100), Phys. Rev. Lett. 66 (1) (1991) 72.
[35] J. Goniakowski, F. Finocchi, C. Noguera, Polarity of oxide surfaces and nanostructures, Rep. Prog. Phys. 72 (1) (2007) 016501.
[36] E.K.K. Abavare, J.-I. Iwata, A. Oshiyama, Atomic reconstruction and electron states at interfaces between 3 C-SiC (111) and Si (110), Phys. Rev. B 87 (23) (2013) 235321.
[37] P. Hohenberg, W. Kohn, nhomogeneous electron gas, Phys. Rev. 136 (3B) (1964) B864.
[38] W. Kohn, L.J. Sham, Self-consistent equations including exchange and correlation effects, Phys. Rev. 140 (4A) (1965) A1133.
[39] J.P. Perdew, A. Zunger, Self-interaction correction to density-functional approximations for many-electron systems, Phys. Rev. B 23 (10) (1981) 5048.
[40] D.M. Ceperley, B.J. Alder, Ground state of the electron gas by a stochastic method, Phys. Rev. Let. 45 (7) (1980) 566.
[41] N. Troullier, J.L. Martins, Efficient pseudopotentials for plane-wave calculations, Phys. Rev. B 43 (3) (1991) 1993.
[42] L. Kleinman, D.M. Bylander, Efficacious form for model pseudopotentials, Phys. Rev. Lett. 48 (20) (1982) 1425.
[43] G. Theodorou, G. Tsegas, Theory of electronic and optical properties of 3C-SiC, J. Appl. Phys. 85 (1999) 2179.
[44] Y. Gao, F. Zhang, W. Zhang, The electronic and structural properties of 3C-SiC: a first-principles study, Adv. Mat. Res. 971 (2014) 208.
[45] W.R.L. Lambrecht, B. Segall, M. Methfessel, M. van Schilfgaarde, Calculated elastic constants and deformation potential of cubic SiC, Phys. Rev. B 44 (8) (1991) 3685.
[46] J.R. Chelikowsky, N. Troullier, Y. Saad, Finite-difference-pseudopotential method: Electronic structure calculations without a basis, Phys. Rev. Lett. 72 (8) (1994) 1240.
[47] K. Hirose, T. Ono, Y. Fujimoto, S. Tsukamoto, First-Principles Calculations in Real-Space Formalism, Imperial College Press, London, 2005.
[48] J.-I. Iwata, K. Shiraishi, A. Oshiyama, Large-scale density-functional calculations on silicon divacancies, Phys. Rev. B 77 (11) (2008) 115208.
[49] J.-I. Iwata, D. Takahashi, A. Oshiyama, T. Boku, K. Shiraishi, S. Okada, K. Yabana, A massively-parallel electronic-structure calculations based on real-space density functional theory, J. Comput. Phys. 229 (6) (2010) 2339–2363.
[50] Y. Hasegawa, J.-I Iwata, M. Tsuji, D. Takahashi, A. Oshiyama, et. al., in: Proceedings of 2011 International Conference for High Performance Computing, Networking, Storage and Analysis (SC2011) (ACM, NY, USA).
[51] The formation energy here is defined as the energy gain in forming 3C-SiC from crystalline Si and diamond; 2013.
[52] E. Greenberg, C.A. Natke, W.N. Hubbard, J. Chem. Thermodyn. 2 (2) (1970), 193–20.
[53] Norm-conserving pseudopotentials of hydrogen are generated using Troullier-Martins scheme and the calculated bond lengths of Si-H in silane and C-H in methane are confirmed to agree with the experimental values within −0.146 %, and −0.003%, respectively. In the slab models we consider, hydrogen atoms are attached with either Si or C atoms of the outermost layers with the above corresponding bond lengths.
[54] S.T. Pantelides, Defects in amorphous silicon: A new perspective, Phys. Rev. Lett. 57 (23) (1986) 2979.